September 2013

Three-Dimensional Modeling of Chicken Anemia Virus VP3 and Porcine Circovirus Type 1 VP3

Curtis James Innamorati
Worcester Polytechnic Institute

Lee Frank Hermsdorf-Krasin
Worcester Polytechnic Institute

Samuel Casey Eisenberg
Worcester Polytechnic Institute

Three-Dimensional Modeling of Chicken Anemia Virus VP3 and Porcine Circovirus Type 1 VP3

A Major Qualifying Project

Submitted to the faculty of

WORCESTER POLYTECHNIC INSTITUTE

in partial fulfillment of the requirements for the Degree of Bachelor of Science in Biochemistry and Chemistry by:

_____

Sam Eisenberg

_____

Lee Hermsdorf-Krasin

_____

Curtis Innamorati

September 12th, 2013

Approved:

_____

Dr. Destin Heilman, Advisor

Department of Chemistry and Biochemistry, WPI

Abstract

The third viral protein (VP3) of the Chicken Anemia Virus (Apoptin) and Porcine Circovirus Type 1 (PCV1VP3) have potential therapeutic cancer killing properties. Though advances have been made in understanding their apoptotic mechanisms, the reasons behind their cancer cell selectivity have thus far eluded researchers. Further, researchers have been unable to isolate and crystallize these proteins, and this lack of a known structure greatly contributes to the difficulty of studying their selectivity. In the past decade protein prediction algorithms have made great strides in the ability to accurately predict secondary and tertiary structures of proteins. This project aimed to generate possible functional models of these proteins using the available prediction techniques. One significant and well defined function of these proteins is their ability to specifically localize to the cell nucleus or cytoplasm. In order to link and evaluate the results generated from tertiary structure predictions with possible mechanisms for localization, experiments regarding the activity of nuclear export signals in the proteins were performed. The generated models strongly suggest that a conformational change plays a significant role regarding the localization of Apoptin and that the export capabilities of PCV1VP3 are CRM1-dependent.

Acknowledgements

We would like to thank Dr. Destin Heilman for his constant guidance and patience throughout this project. We would also like to thank Victoria Huntress for helping us with imaging for this project. We would like to thank the Foldit team at Baker laboratories and the Foldit players for contributing their time to the development of three-dimensional models for Apoptin.

Table of Contents

Background

The Circoviridae viral family consists of small, icosahedral, non-enveloped virions with circular, single-stranded DNA (ssDNA) genomes and has likely been existent for more than 40 million years[3]. Two species of virus in this family, the Chicken Anemia Virus (CAV) and the Porcine Circovirus type 1 (PCV1), are of particular note due to their potential as anti-cancer agents: the third viral proteins (VP3) of both CAV and PCV1 (labeled Apoptin and PCV1VP3, respectively) have the ability to induce apoptosis in transformed cells while leaving primary cells unharmed, though the exact mechanism by which these proteins work remains unknown[6,35,61]. A number of studies have been conducted on Apoptin[11,12,13,20,21,52]. PCV1VP3 has been studied much less extensively.

Both CAV and PCV were first described in the 1970s. In 1979, N. Yuasa *et al* described an agent causing severe anemia in chicks that were offspring of chickens treated with a contaminated Marek's disease vaccine[59]. These experiments showed 100% morbidity in 1-day old chicks, but very low infection and fatality rates for chicks older than 1 week, even though the infectious agent was still present in these older subjects[59]. Later studies into the agent, the Chicken Anemia Virus, show that it can act in tandem with other infections to cause profound immunosuppression, and that it can be transmitted vertically, from hen to chick, causing severe anemia in progeny[48].

The Porcine Circovirus was first described in 1974 as a contaminant in the PK-15 porcine kidney cell line[56]. There are two major serotypes of PCV, 1 and 2, the former being non-pathogenic[34]. While PCV1 is considered non-pathogenic, PCV2 is the causative agent of Post-Weaning Multisystemic Wasting Syndrome (PWMS) in young pigs[18]. PWMS symptoms include weight loss, lesions on internal organs, lymphocyte depletion, neurological disorders, and often

death[4,6]. However, while PCV2 is the pathogenic strain, studies have shown that the VP3 of PCV1 causes more apoptosis in a wider variety of cells[6].

The overall viral structures of PCV1 and CAV are quite similar. Both contain a small circular, ssDNA genome with 3 overlapping Open Reading Frames, or ORFs, and in each virus the products of ORFs 1 and 2 are required for infection, structure, and replication[1,33,35,40,41,48,61]. In CAV, ORF1 codes for the largest protein (51.6kDa) and is thought to make up the entirety of the capsid protein, while ORF2 codes for a 24kDa protein that has a number of functions, including the facilitation of replication and capsid creation[1,7,41]. ORF1 of PCV1 codes for two replication proteins, *rep* and *rep'*, the latter being a truncated copy of the first, while ORF2 creates the major capsid protein, *cap*[35,40]. For both PCV1 and CAV, ORF3 codes for a protein that is not required for replication or structure, but appears to be associated with viral pathogenesis[33,61]. Studies have shown that the third viral protein from both viruses (labeled Apoptin for CAV and PCV1VP3 for PCV1) selectively target transformed cells for apoptosis, however the actual properties and actions of the VP3 differ between each virus.

PCV1VP3 is almost twice the length of Apoptin (206aa compared to 121aa) and has a much less well-defined apoptotic pathway[6,52]. The only data known regarding PCV1VP3's mechanism of apoptosis is that it is caspase-dependent[6]. On the other hand, it is known that Apoptin causes apoptosis through a p53-independent pathway and G2/M arrest. The C-terminus of Apoptin binds to APC1, the largest subunit of the Anaphase Promoting Complex/Cyclosome (APC/C), and sequesters APC1 into PML bodies where it is rendered inactive[20,52]. These PML bodies are not normally present in the cell during the G2/M phase, and are thought to also be caused by Apoptin. Inhibition of the APC/C complex and the formation of PML bodies leads to G2/M cell cycle arrest and eventually results in apoptosis through a p53-independent pathway[52].

While the full extent of this apoptotic pathway is unknown, several parts have been elucidated. It is know that Apoptin uses an intrinsic mitochondrial pathway dependent on caspases 3 and 9[37]. The pathway is typically triggered by hypoxia, DNA damage, nitric oxide, Ca^{2+} fluctuations, cellular stress or proteases[2]. These factors activate members of the Bcl-2 protein family, which increase the permeability of the outer mitochondrial membrane and lead to the release of Cytochrome-C into the cytosol[8]. Cytochrome-C creates the apoptosome and this activates caspase-3 via caspase-9, which proceeds to degrade the cell[2,16, 22].

In addition to the differences between apoptotic pathways, Apoptin and PCV1VP3 show different cellular localization. Apoptin localizes to the nucleus in transformed cells, but to the cytoplasm in primary cells[13]. A study by Heilman *et al* showed that Apoptin's unique nucleocytoplasmic shuttling is the result of a CRM1-dependent Nuclear Export Sequence (NES) between residues 33-46 and an active bipartite Nuclear Localization Sequence between residues 70-121[20]. The NES in particular is a canonical CRM1 sequence, IAGITITLSL, which follows the pattern Φ-X-$_{2\text{-}3}$- Φ -$X_{2\text{-}3}$- Φ -X- Φ, where Φ represents I, L, F, V, or M and X represents any other amino acid[15]. Mutation of Leu44 and Leu46 to Alanine eliminates Apoptin's cytoplasmic localization in primary cells, implying that the NES is functional, while treatment of Apoptin infected primary cells with Leptomycin B also causes nuclear accumulation, implying that the NES is Crm1-dependent[20]. Interestingly, inducing the localization of Apoptin to the nucleus is not sufficient to cause apoptosis by itself. Data from the same paper imply that the NES is involved with Apoptin's multimerization capabilities. The multimerization sequence was mapped to the same area in the N-terminus as the NES, and when the sequence was mutated or removed, Apoptin lost all localization specificity in both primary and transformed cells, as well as the ability to cause apoptosis[20]. The source of the difference in Apoptin's localization between

primary and transformed cells is unknown, however it is thought to be associated with Apoptin's propensity to multimerize with itself as large 30-40 monomer subunits[28].

Unlike Apoptin, PCV1VP3 localizes to the cytoplasm in both primary and transformed cells[46]. However, a recent study implies that PCV1VP3 may have a large degree of homology with Apoptin in terms of structural motifs of both the NES and NLS[51]. A putative NES is located between residues 42-49 and a putative NLS between residues 80-105[46]. Our colleagues also predicted a very strong NES in the tail domain of PCV1VP3 at residues 134-149, which might help explain the proteins strong cytoplasmic localization[9]. Interestingly, the study was unable to eliminate the cytoplasmic localization of the protein through site-directed mutagenesis of the putative NES in both the primary and tail sequences, implying that the localization could be caused by some other factor or a non-classical NES[9].

While little else is known about PCV1VP3, there have been numerous papers examining possible interactions with Apoptin in an attempt to elucidate the reason behind its selectivity for transformed cells. Beyond APC1, studies have shown that Apoptin can directly interact with double-stranded DNA, though the reason for this interaction is unknown, and the regulatory subunit of PI3K, resulting in the activation of PI3K and the continuous activation of Akt[28,29,30,36,39]. One of the largest debates surrounding Apoptin is the differences in phosphorylation between primary and transformed cells, specifically Threonine 108. It has been shown that T108 is phosphorylated by CyclinA-CDK2 in transformed cells, and a study researching a mutant that simulated the phosphorylation of T108 reported that this caused nuclear localization and apoptosis in primary cells[38,47]. However, multiple studies have since shown that the phosphorylation of T108 has no effect on the activity of Apoptin and is unnecessary for the nuclear localization or induction of apoptosis in transformed cells[19,24,27].

A recent study by Kucharski *et al.* implies that the DNA Damage Response (DDR) signaling pathway may play a crucial role in Apoptin's selectivity[24]. Their results show that inducing DNA damage in primary cells via Bub1 knockdown or treatment with bleomycin caused Apoptin to localize to the nucleus, whereas blocking DDR signaling in transformed cells with caffeine caused Apoptin to localize to the cytoplasm and lose its apoptotic ability. The research further showed that Apoptin could be localized to the cytoplasm by the inhibition of two key kinases in the DDR signaling pathway, ATM and DNA-PK.

The main problem with both Apoptin and PCV1VP3 is that attempts to elucidate their structure through traditional methods such as x-ray diffraction crystallography have been unsuccessful due to the proteins' small size and Apoptin's tendency to multimerize. The homology testing conducted by our colleagues took only the primary sequence of each protein into account, which is likely not representative of the actual protein structure[51]. In order to better understand the structure-function relationship of both PCV1VP3 and Apoptin, it is necessary to find a method to elucidate the proteins secondary and tertiary structures.

A relatively recent alternative to traditional structure analysis methods is in silico tertiary protein structure prediction, which has begun to garner much interest due to the incredible increases in computing power. Modern supercomputers are more than capable of crunching the algorithms required for protein prediction and, additionally, some research teams have developed a distributive computing model that crowd-sources the computations to computers connected to a central network. One example of this is the program Rosetta@home developed by David Baker's lab at University of Michigan[14] in which a user can download a program that will crunch an algorithm with their computer's idle processing power.

While people have approached protein modeling in several ways, most modern programs use a method called Ab Initio modeling. The most common first step in computational protein modeling is an attempt to determine the protein's secondary structure via homology modeling. One such method is NCBI's Basic Local Alignment Search Tool, or BLAST which looks for regions of local similarities between the primary sequences of a protein with an unknown structure and a protein with a known structure, and then determines if those similarities are statistically significant. However, a protein may not always have a homologue with known structure to compare it to, in which case the algorithm uses protein threading to determine its secondary structure. Protein threading operates under the assumption that there exist a limited number of basic folds in nature, so it attempts to fit, or "thread" the primary sequence of the unknown protein onto the secondary structure of known proteins and then quantifies whether the new secondary structure of the unknown is allowed based on amino acid size, Van der Waals interactions, and hydrophobicity.

Determining a hypothetical secondary structure greatly decreases the number of possible configurations for a protein's tertiary structure into a more manageable pool. Knowing the location of the protein's alpha helices and beta sheets gives the backbone some rigidity, and this is vital for the next step in the folding algorithm, which involves moving the backbone around using a "random walk" method. By far the most efficient method for this step involves a Metropolis Monte Carlo algorithm[31]. First, the computer calculates the free energy (E_1) of a random 3D configuration. Then, it moves a single amino acid a certain distance, based on a defined temperature of the model, in a random direction and recalculates the free energy (E_2). If the energy of the system is lower in the new configuration, then the move is accepted and the process repeats from the new configuration. If the energy of the system is higher, the algorithm

does not immediately reject the move, but first checks if that energy state is an intermediate by searching for a nearby lower energy state. It evaluates each move using the function:

$$\mathbf{F(T)=exp(-\Delta E/kT)}$$

where k is the Boltzmann constant and a random number R where $0<R<1$. If $F(T)>R$, the move is accepted, and if $F(T)<R$ the move is rejected. The online program I-TASSER, developed by the Zhang Lab, takes this algorithm a step further using a Replica Exchange Monte Carlo, or REMC, algorithm that takes advantage of the fact that the move evaluation function is based on temperature[26]. It starts with an elevated temperature, which results in more rejected energy states, but randomly switches to both lower and higher temperatures. This results in a much larger spread of energy models using approximately the same amount of computing power as a single temperature Monte Carlo simulation.

There exists a biennial assessment of tertiary prediction algorithms which is used as a standard for ranking the accuracy of these algorithms. The Critical Assessment of Protein Structure Prediction (CASP) tests the accuracy of these algorithms by providing research groups with a chance to predict a protein's tertiary structure before its actual structure, as determined by x-ray diffraction or NMR spectroscopy, is released.

Materials & Methods

3D Prediction Methodology

For this project the sequence of the Japanese 82-2 isolate of Apoptin was used for structure prediction (Entry VP3_CAV82 on Uniprot, Taxon ID 73476). Multiple programs and algorithms were used in the analysis of Apoptin and PCV1VP3. Initially primary sequences for Apoptin and PCV1VP3 were submitted in FASTA format to the Raptor-X, I-TASSER, QUARK, and ROBETTA servers for tertiary structure prediction. While these programs also perform secondary structure prediction, independent secondary structure prediction was carried out on Apoptin and PCV1VP3 using PSIPRED. Additionally, YASPIN and GOR were also used with Apoptin. I-TASSER also returned predictions on solvent accessibility.

The primary sequence FASTA for Apoptin was submitted to the Fold It team at The Baker Lab along with the top 5 predicted Zhang models as a template. The puzzle was posted for 1 week during which players attempted to manually lower the free energy of the protein models through manipulation of the backbone and sidechains. When the puzzle was closed, we received the top 10 scoring models found by the players.

Swiss PDB Viewer

Several tools in Swiss PDB Viewer (Deep View) were used for qualitative and quantitative analysis. For simple alignment a .pdb file of the x-ray diffraction crystallography of the Nuclear Export Signal from HIV-Rev and PKI alpha bound to the CRM1/RanGTP complex were imported into Deep View. The actual HIV-Rev NES as well as the PKI alpha NES were isolated by selecting the actual NES sequence, inverting selection (alt+1), and removing the unwanted, now selected residues (Build → Remove Selected Residues.) The resulting file was

saved. The Apoptin models predicted by I-TASSER, ROBETTA and Foldit were imported into Deep View and the NES was similarly isolated. An attempt was then made to align the critical leucines between each NES using Deep View's alignment tools, “Magic Fit,” and “Fit Molecules (from selection).” The force field energies for all mentioned models were calculated using the “Compute Energy (Force Field)” tool.

Cell Culture Maintenance

H1299 non-small human lung carcinoma cells were maintained in Dulbecco’s Modified Eagle Medium (DMEM)/High Glucose, 10% fetal bovine serum (FBS), and PSF (100 units/mL Pen G sodium; 100mg/mL streptomycin sulfate; 0.25 mg/mL amphotericin B). Cells were incubated at 37°C and 5% CO2 humidity. Confluence was maintained below 95% by means of frequent passage. In order to pass cells, media was aspirated and cells were washed with 10mL of 1X PBS followed by aspiration and addition of 2mL trypsin. Trypsin was aspirated and cells were observed for movement. Once movement was observed, cells were washed vigorously with 10mL of fresh media until re-suspension occurred. 2mL of this re-suspension was added to a new 75 square cm tissue culture flask, in addition to 10mL fresh media. The cells were allowed to grow to 95% confluence before passing again.

Plating of 6 well plates

Square Coverslips were washed in 100% ethanol, added to each well, and allowed to dry. When a 75 square cm tissue culture flask reached 95% confluence, cells were passed into a new 75 square cm tissue culture flask, following the procedure outlined in cell culture maintenance. 8 mL of media and cells was taken from the original flask, added to a 50 mL conical tube and diluted with 17 mL of fresh media making an approximate ⅓ dilution. This was then added to

each well in 2 mL increments. Cells were allowed to grow to 75% confluence before transfection occurred.

Transfection

H1299 cell lines were transiently transfected with CAV VP3, PCV1 VP3, and PCV1 Tail (a.a. 105-206). All mutants were N-terminally tagged with GFP and contain a vital CMV promoter region, which was used to control transfection using Effectene Transfection Reagent Kit by Qiagen. Transfection occurred when cells were approximately 75% confluent. Media was aspirated from 6 well plates, wells washed with 1X PBS, each well received 1.6 mL of fresh media. Plasmid DNA was added using, 2 µL for Apoptin constructs and 4 µL for PCV1 constructs, diluted with EC buffer to a final volume of 200 µL. 6.4 µL of enhancer was added, briefly vortexed, and allowed to incubate at room temperature for 2-5 minutes, followed by the addition of 20 µL of Effectene reagent. The samples were incubated at room temperature for 5-10 minutes to allow for complex formation to occur. 1.2 mL of media was added to the complexes, gently mixed by pipetting, and approximately 710 µL was immediately added dropwise to each well. Plates were gently swirled and incubated and at 37°C and 5% CO2 humidity.

Leptomycin B Experiments

Leptomycin B was obtained from Sigma-Aldrich at a concentration of 5.5 µg/mL in a 7 to 3, methanol to water ratio. Leptomycin B was stored at -20 °C as per directed by the MSDS. H1299 cells were transfected following the outlined transfection procedure. Twenty-four hours post transfection media was aspirated and control samples were replaced with 2 mL of fresh media. To obtain a working concentration of 2.5 ng/mL, 7.3 µL of stock leptomycin B was

added to 16 mL of media, and 2 mL of this was quickly added to each well. Eight hours post addition cells were fixed following the preservation of 6 well plates procedure outlined below.

Preservation of 6 well plates

Post transfection and addition of various inhibitors, the cells were fixed and preserved. The media was aspirated and cells washed with 2mL 1X PBS and aspirated to remove residual media. Approximately 1mL of a 4-fold dilution of 10mL paraformaldehyde diluted in 30mL 1X PBS was added to each of the wells before gentle agitation for 15 minutes. The PBS with 4% paraformaldehyde was aspirated and the cells washed with 2mL PBS. To preserve and sterilize coverslips 70% ethanol was added to each well and plates were stored until mounting.

Mounting Procedure

Coverslips were mounted to slides in order to be viewed under confocal microscopy. Approximately 30µL of mounting media (50% glycerol; 100 mM Tris (pH 7.5); 2% DABCO, 10µg/mL DAPI) was added to each slide. Coverslips were taken out of 70% ethanol and allowed to air dry before placing onto slides. Coverslips were pressed to remove excess mounting media, sealed with nail polish, and allowed to dry before storing.

Quantification of Cellular Location

Three fields of view of H1299 cells transfected with GFP-tagged PCV1 and treated with leptomycin B were taken at 40X magnification. These fields of view were used to quantify the location of GFP-tagged PCV1 within the cells. These fields of view were compared against two fields of views of cells which did not contain leptomycin B. Statistical analysis was performed to determine if the addition of leptomycin B has a statistical effect on the localization if PCV1.

Nuclear/ Cytoplasmic Fraction Determination

The software ImageJ was used to calculate the nuclear/cytoplasmic ratio for the GFP-tagged PCV1 construct and the GFP-tagged PCV1 tail mutant construct. The fluorescent intensity of GFP located in the nucleus and cytoplasm was calculated for three representative cells containing leptomycin B and three representative cells without leptomycin B. The corrected total cell fluorescence (CTCF), calculated by integrated density - (area of selected cell X mean fluorescence of background reading), was used to graphically show the nuclear/cytoplasmic ratio.

Using the plot profile function and the line tool in Image J, a brightness intensity plot was created. A distance from the inner nuclear membrane to the outer cell membrane was measured and the brightness intensity was graphically determined for each point on the line. Two graphs were created one using a representative cell treated with leptomycin B and the other using a representative cell in the absence of leptomycin B.

Preparation of CDC25 Inhibitor NSC 95397

NSC 95397 was obtained from Sigma-Aldrich; it has a solubility of 16mg/ml in Dimethyl Sulfoxide (DMSO), and was stored at -20˚C as per directed in the MSDS. To prepare a 32 mmol stock solution 1 mg of NSC 95397 was dissolved in 100 µL of DMSO and vortexed. To get the desired working concentrations 1 µl of the stock solution was dissolved in 999 µl DMSO to make a 32 µmol solution. Addition of NSC 95397 occurred 4 hours post transfection. In one 6-well plate containing GFP-Apt transfected cells we prepared wells with working concentrations of 0 nmol, 32 nmol and 128 nmol NSC 95397 in duplicate by adding 0 µL, 2 µL and 8 µL of the 32 µmol NSC 95397 solution to the wells. Cells were then fixed 24 hours post transfection following the preservation of 6 well plates procedure outlined.

Results

The functionality of proteins is determined by their tertiary structure, so it is important to develop accurate models to further investigate these cancer killing proteins. The traditional methods of determining protein structure such as x-ray diffraction crystallography do not work for Apoptin and PCV1VP3 due in part to their inability to be crystallized. As an alternative, protein structure prediction programs were used to elucidate the tertiary structures of Apoptin and PCV1VP3. The current top three tertiary prediction programs (as of 2012) as ranked by CASP were I-TASSER, QUARK, and ROBETTA, all of which were utilized for this project. In addition the team at Baker Laboratories was consulted to use their distributed manual prediction program Foldit, because while the former three programs are powerful and accurate they have faults which can't be solved through random walk algorithms. The structure prediction programs returned a variety of models for both proteins, and some common motifs between prediction models were apparent.

For Apoptin there was good consensus between all programs that the C-terminus, the location of the bipartite NLS sequence, was mostly helical. However, there was discrepancy on the structure of the hypothesized NES region. The secondary prediction algorithm PSIPRED as well as the secondary structure prediction algorithms built into I-TASSER, QUARK and ROBETTA all predicted two anti-parallel beta-sheets with a hairpin turn; however, Foldit players returned lower energy conformations that had no definite structures in the NES region. **Figure 1** displays models of Apoptin generated from ROBETTA, Foldit, I-TASSER and QUARK. The models show that the critical residues necessary for nuclear export (displayed in black) are predicted to be buried and not accessible. Additionally proteins with a higher homology rating were used to predict a tertiary structure for Apoptin by restricting I-TASSER to

templates with 20% or higher similarity. In both the top-scoring Foldit model and the I-TASSER 20% homology cutoff model the critical leucine residues, L44 and L46, are positioned trans to each other. Overall, the programs predicted that Apoptin is mostly highly disordered coil, which is consistent with previous experimental data[30].

Having confidence in these prediction programs prompted the exploration of PCV1VP3. The I-TASSER, ROBETTA and PSIPRED algorithms were used to determine tertiary and secondary structure for PCV1VP3. There was strong confidence that the tail region of PCV1VP3 was almost entirely made up of hydrophobic helix, in fact all 3 programs predict 5 distinct typical helixes. Further, ROBETTA predicted that PCV1VP3 contains two separate domains: the first consisting of amino acids 1-104 and the second consisting of amino acids 104-206. **Figure 2** depicts models of PCV1VP3 generated from ROBETTA and I-TASSER, including 2 models in which the tail region (a.a.'s 104-206) were isolated and predicted as stand alone proteins. All prediction programs describe the putative NES in PCV1VP3 as located in a region with a high confidence in structure. This region is also located in an accessible area of the tail which lies on a surface helix. If the putative NES in the tail region of PCV1VP3 can assume a conformation that is consistent with the location of the critical residues of a known CRM1-dependant NES, it is possible that the PCV1VP3 NES could bind to CRM1.

A possible method to test if the PCV1VP3 NES can bind to CRM1 is to compare it with known NES structures. HIV-Rev and PKI alpha both contain canonical CRM1-dependent nuclear export sequences. Further, their NES have been crystallized and their structures are known. The critical residues in the export sequences of HIV-Rev and PKI alpha align well. It is plausible that if the predicted structure of the tail region NES in PCV1VP3 is similar to the NES in these known proteins, then the PCV1VP3 NES could be functional. Deep View was used to

isolate the NES in PCV1VP3 and compare it to the known crystallized NESs HIV-Rev and PKI alpha. “Fit” tools in Deep View, specifically “Magic Fit” and “Fit Molecules (from selection)” as well as the align tool in the top menu were used for this comparison. Representations of the crystallized structure of the HIV-Rev NES and PKI alpha NES are shown in **Figure 3**. Simple observation was used to qualitatively determine that it was possible for the critical NES residues in PCV1VP3 to align with the critical residues in HIV-Rev. **Figure 4** is a crystallization of HIV-Rev bound to CRM1. **Figure 5** shows that the critical residues in the HIV-Rev NES occupy a similar spatial arrangement as hydrophobic residues located in the putative PCV1VP3 NES. These residues could potentially bind the CRM1 pocket. This could be tested by modifying the activity of CRM1.

Leptomycin B, a suicide substrate inhibitor of CRM1 that binds into the active pocket of CRM1 and covalently modifies a critical residue, Cysteine 528, is the current standard for testing whether nuclear export is CRM1-dependent. To test whether the cytoplasmic localization of PCV1VP3 is caused by a CRM1-dependent NES, several experiments were conducted with PCV1VP3-transfected cells and leptomycin B. Visualization of cells transfected with GFP-tagged PCV1VP3 shows nuclear accumulation in cells treated with leptomycin B and cytoplasmic localization in the control cells without leptomycin B (representative cells shown in **Figure 6**). Qualitative analysis of PCV1VP3 cell images showed that 56% of transfected cells treated with leptomycin B favored nuclear accumulation, while in comparison only 35% of transfected cells without leptomycin B favored nuclear accumulation. A Student T test determined that the results are statistically relevant at 90% confidence (p-value=0.10). The increase in nuclear accumulation for cells treated with leptomycin B implies that the nuclear export capability of PCV1VP3 is affected by leptomycin B, and thus CRM1 dependent.

To quantitatively determine whether there was a significant difference between the localization of PCV1VP3 in cells treated/untreated with leptomycin B, a treated and untreated representative cell was analyzed. More specifically, ImageJ, an image analysis program, was used to generate graphs which examine the fluorescence of GFP in both the cytoplasm and nucleus. The plot profile function of ImageJ was used to create an intensity plot which graphically quantifies fluorescence results, in order to remove any possible bias in the visualization of results. Given an image of a cell visualized with confocal microscopy, ImageJ determines the brightness intensity of the GFP expressed in different areas of the cell based on a pixel's 8 bit greyscale value. Brightness intensity graphs were made for representative cells in the presence of leptomycin B and in the absence of leptomycin B, and are shown in **Figure 7**. In the absence of leptomycin B, the brightness intensity graph shows much greater cytoplasmic fluorescence intensity than nuclear fluorescence intensity. Cells treated with leptomycin B show an equal distribution of fluorescence intensity in both the cytoplasm and nucleus. Results indicate that graphically there is a difference between the localization of GFP- tagged PCV1VP3 when treated with leptomycin B and in the absence of leptomycin B, further evidence that PCV1VP3 is sensitive to leptomycin B and has some dependence on CRM1-mediated export.

To further quantify the results obtained from the brightness intensity graph, Image J was used to calculate the corrected total cell fluorescence, of representative cells, to determine the ratio of GFP intensity in the nucleus compared to GFP intensity in the cytoplasm, i.e. the nuclear/cytoplasmic ratio. **Figure 6** displays a graphical representation of the ratio for the representative cells treated with and in the absence of leptomycin B. Cells treated with leptomycin B showed an 81% nuclear to 19% cytoplasmic fluorescence intensity, while cells without leptomycin B showed a 23% nuclear to 77% cytoplasmic fluorescence intensity. A

student T test determined that the results are statistically relevant at 95% confidence (p-value=0.047). We can therefore reject the null hypothesis that leptomycin B has no effect, which further supports that PCV1VP3 has a CRM1-dependent NES.

A construct containing just the tail region of PCV1VP3 was also treated with leptomycin B, however the results were inconclusive. Full-length PCV1VP3 was used as an internal control for the experiment, since it had previously been shown to be leptomycin B-sensitive. However, in this experiment no effect on the full-length PCV1VP3 was observed, implying that the leptomycin B stock was no longer active. Due to time constraints, this experiment could not be repeated. Under confocal microscopy the PCV1 tail mutant showed strong cytoplasmic localization. Punctate expression of GFP could be seen under the confocal microscope. Further experimentation must be performed before ruling out the presence of a functional export sequence in the tail region of PCV1.

In a follow up to a recent study into the effects of the DNA Damage Response pathway on Apoptin, the effects of one specific phosphatase involved in the DDR pathway, CDC25a, was tested with Apoptin. Apoptin-transfected cells were treated with a CDC25a inhibitor, NSC 95397; however, no change in Apoptin's localization was observed (data not shown). Knowing from Kucharski *et al* that Apoptin is influenced by an agent downstream of ATM and DNAPK in the DDR pathway, this data implies that the effector is either located between ATM/DNAPK and CDC25a or on a different branch of the pathway. Further experimentation into the relationship between Apoptin's activity and the DNA Damage Response pathway needs to be conducted.

Discussion

Knowing the structure of a protein, even a theoretical one, can be a great aid in determining the protein's function or in supporting data that imply a certain section of the protein has a specific function. Apoptin has been shown to contain a functional, CRM1-dependent NES sequence between residues 33-46. However, all predictions performed present these residues with very low solvent accessibility, implying that the NES is buried in Apoptin's lowest energy state. Two possible conclusions can be drawn from these results: either the predicted structures are reflective of reality and a conformational change is necessary to expose the critical residues that allow for the CRM1-NES complex to form, or the three dimensional predictions are not reflective of reality. While it is true that three-dimensional predictions are prone to error, they are, at the very least, decent guesses that reflect larger protein folding motifs. Even if the software has very low confidence in the predicted structure, the general shape of the protein can still be seen as an estimate of reality. When combined with the fact that the pattern with Apoptin was consistent across all prediction programs, it is more likely that this motif is a significant approximation of reality. Thus, the results imply that Apoptin's nuclear export capabilities are mediated by a conformational change. This change could be associated with multimerization, protein modification such as phosphorylation, or a combination of the two. Previous research has suggested that the shuttling capabilities of Apoptin may be mediated through phosphorylation; however there is no consensus thus far.

To examine whether phosphorylation of Apoptin could result in a conformational change, multiple mutants were submitted to I-TASSER with Serines/Threonines mutated to Glutamic Acid in order to simulate a phosphorylated group. The NetPhos server, which predicts Serine/Threonine and Tyrosine phosphorylation sites in proteins, was used to determine which

amino acids to mutate. Unfortunately, the results were inconclusive: while conformational changes were observed, none appeared to completely expose the NES. Predictions were not run with combinations of phosphorylation sites so further testing is suggested, however it is important to keep in mind 3D predictions are still simply best guesses and that our current best models are still of low confidence because of a complete lack of known homologue structures. Very interesting results were received from running a prediction on one of the more noteworthy Apoptin point mutations, changing leucines 44 and 46 to alanine, which ablated NES functionality (**Figure 8**). The protein structure completely changed, effectively turning inside out. This lends a bit more confidence to the three dimensional prediction as we know that these mutations completely remove Apoptin's functionality.

A more stringent energy analysis should be performed on these NES regions. One possibility is to use the tools available in Deep View. While basic alignment (i.e. "Magic fit") and observation were used to qualitatively determine whether Apoptin and PCV's NESs are capable of fitting the canonical NES configurations, there is also a "torsion" tool which can physically spin phi and psi angles to effectively thread the NES by hand. This could be used to determine whether the predicted NES could line up with the critical residues of a known, crystallized NES (such as HIV-Rev or PKI alpha). Additional experimental three dimensional analysis techniques that can be used to examine Apoptin and PCV1 include a combination of cryo-electron microscopy and 3D NMR, which may yield a better picture of the larger complexes formed by Apoptin.

The data from both the protein structure predictions and leptomycin B experiments heavily imply that PCV1VP3 has a functional CRM1-dependent NES. When the leptomycin B experiments were repeated for just the tail region of PCV1VP3, which contains a very strong

putative NES, a strong cytoplasmic localization was observed in both cells with and without leptomycin B. However, as stated in the results, this was thought to be an experimental error due to degradation of the inhibitor. Leptomycin B is extremely labile, and undergoes rapid degradation when not stored at -20°C. Even when kept in a cooler for transport and use, it is likely that degradation occurred following several experiments with the same stock. However, it should be noted that confocal microscopy of the tail region of PCV1VP3 showed very punctate GFP expression in the cytoplasm, similar to that of Apoptin in the nucleus of transformed cells (data not shown). These results imply that the isolated tail region of PCV1VP3 could be self-multimerizing or binding to cytoplasmic structures. If these conglomerates reached sizes greater than 40kDa, then they would be unable to passively diffuse into the nucleus and would appear to have a cytoplasmic localization even in the presence of leptomycin B. Further research into the tail region and this interesting phenomenon could help elucidate the structure and function of PCV1VP3.

We suggest that future testing involve imaging the cells sooner after drug treatment and to examine other CRM1 inhibitors such as Ratjadone A, KPT-251, or CRM1 Inhibitor III. Further, experiments should be conducted on the "head" region of PCV1VP3, as well, to determine whether the predicted NES and NLS in that area are functional.

A recent study by Kucharski *et al.* delved further into the protein modification theory by showing that the activation of Apoptin is associated with DNA Damage Response signaling[24]. More specifically, an increase in DDR signaling caused Apoptin to activate and localize to the nucleus, even in primary cells. Combined with our predicted structures, the data implies that Apoptin's NES could be deactivated by a conformational change caused by a component of the DDR signaling pathway. Since our predictions show Apoptin's NES buried at the lowest energy

state, and the NES is typically only active in primary cells, it is possible that Apoptin is actually modified in primary cells and has the modifications removed in transformed cells. This is contrary to much of the previous thought that Apoptin is activated by the addition of a phosphate group in transformed cells, and will require further study into other protein modifiers, specifically those in the DDR pathway.

For this project, we were able to test the effects of one specific phosphatase involved in the DDR pathway, CDC25a, on Apoptin. Inhibiting CDC25a with NSC 95397 failed to relocalize Apoptin to the cytoplasm (data not shown); however, the results are still of interest. If the DNA Damage Response hypothesis is correct then the phosphatase/kinase responsible for Apoptin's shuttling is upstream of CDC25a in the DDR pathway. We suggest repeating the inhibition experiment with a CDC25a inhibition assay to test for chemical activity, as we were unable to perform an assay that tested whether the drug was viable. Also we suggest examining phosphatases/kinases located upstream to CDC25a in the DDR pathway, which will mostly consist of mediators. To test experimentally whether or not a phosphatase is responsible for shuttling in general we suggest testing a general phosphatase inhibitor such as okadaic acid. Additionally, other methods of conformational change could be tested, such as peptidylproly isomerase or related enzymes (PPIL3).

Figures

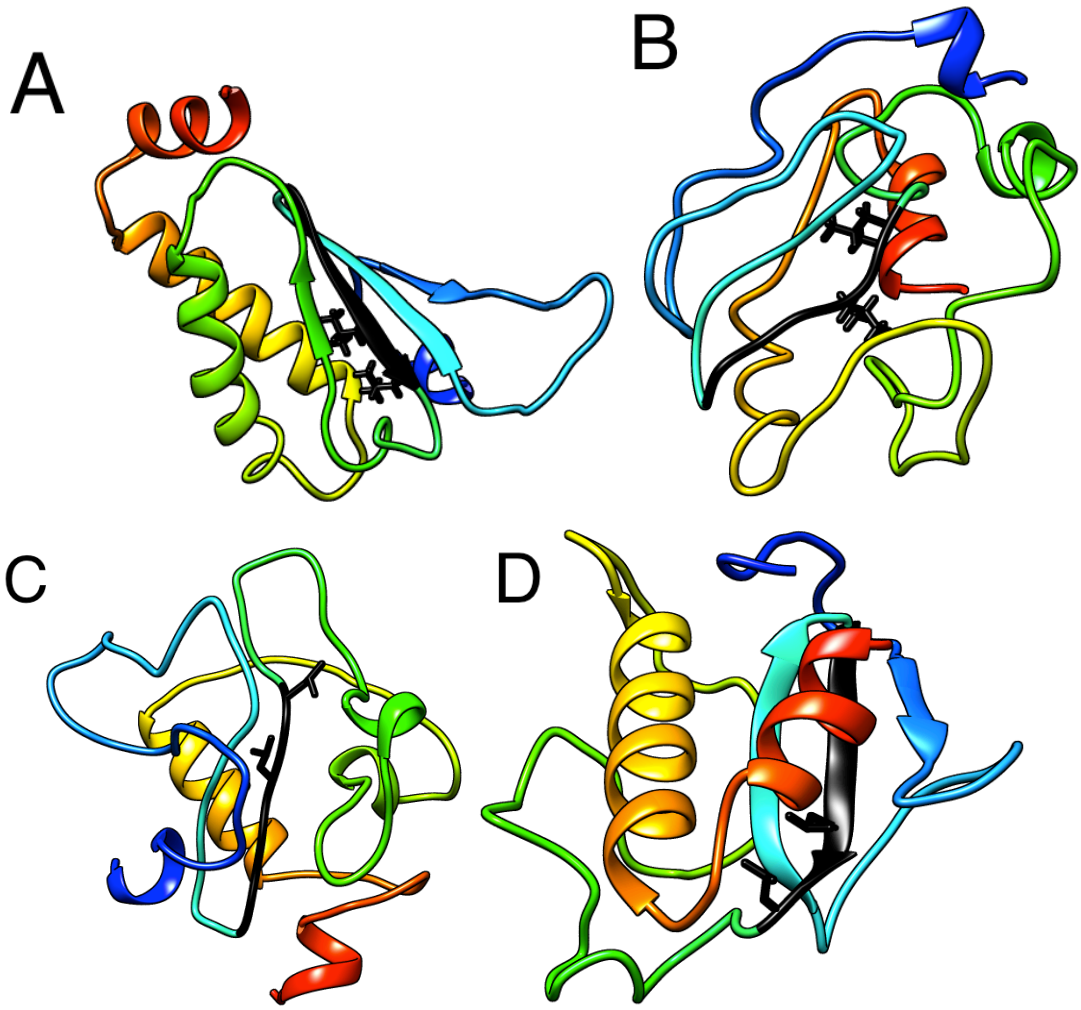

Figure 1: Predicted three dimensional tertiary structure results for Apoptin
In all models the location of the NES is displayed in black, with critical residues Leu44 and Leu46 displayed in atom bond format. All models show that the location of the NES is buried and inaccessible. (A) Tertiary structure was generated from ROBETTA, depicting the location of the NES on an anti-parallel beta sheet. (B) The top-scoring Foldit model depicts a mostly disordered structure. (C) The I-TASSER 20% homology cutoff model depicts a highly disordered protein, consistent with other predictions. (D) Depicts the model generated with QUARK, displaying anti-parallel beta sheets at the NES location. Images were created using UCSF Chimera.

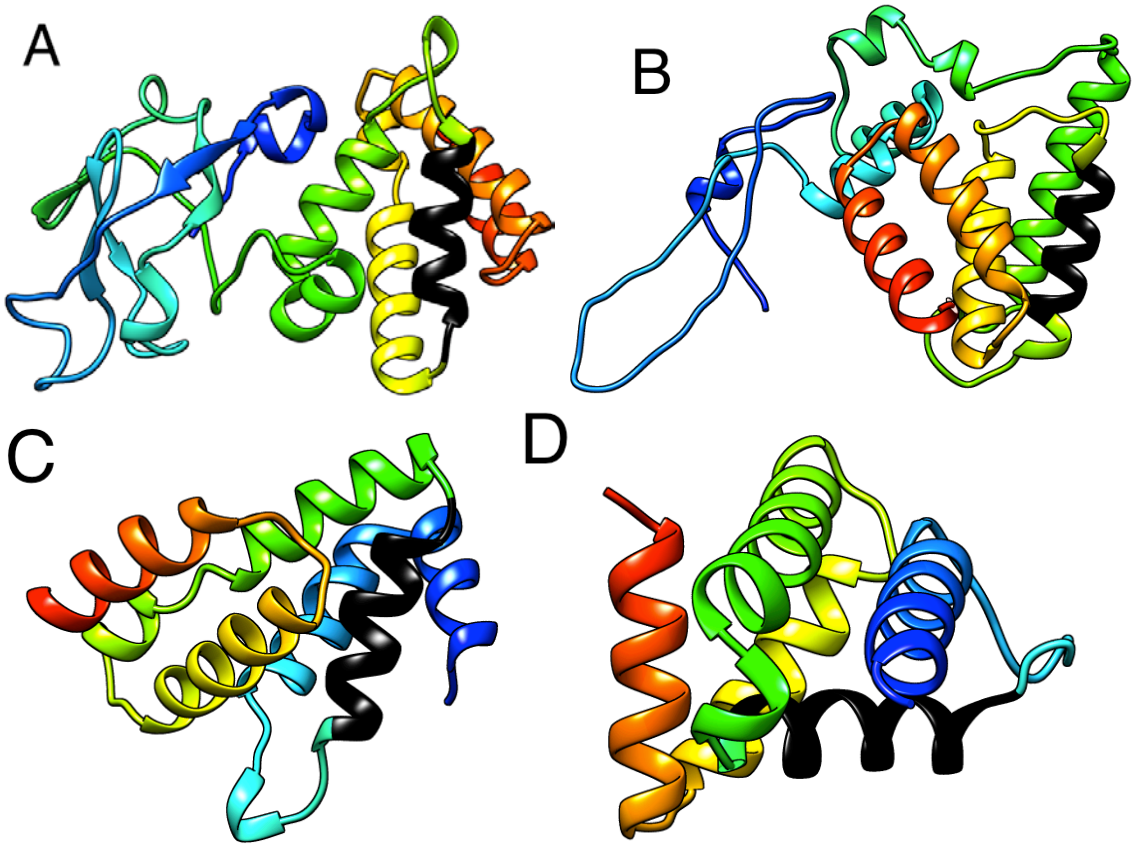

Figure 2: Predicted PCV1 VP3 models from I-TASSER and ROBETTA
(A) A full wtPCV1 VP3 model from ROBETTA, depicting the putative NES in black. (B) Depicts the full wtPCV1 VP3 model from I-TASSER. The putative NES is depicted in black. (C) The results from ROBETTA for the tail domain of PCV1 show similar structure as the full PCV1 domain. The putative NES is displayed in black. (D) The tail domain of PCV1 was isolated and processed by I-TASSER, resulting in 5 hydrophobic helixes. The putative NES is displayed in black. Models were created using UCSF Chimera.

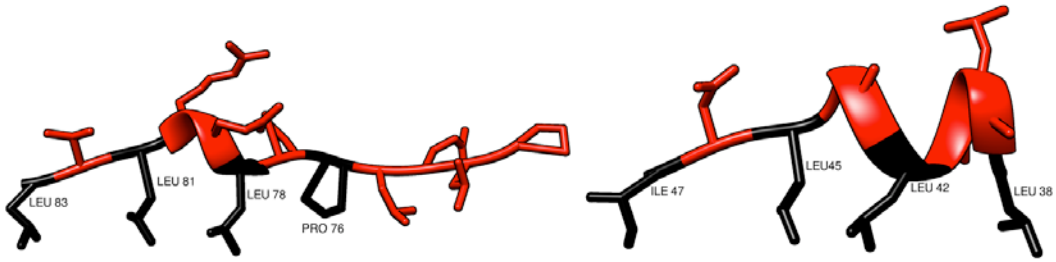

Figure 3: Crystalized structure of known CRM1 dependent NES
Figure 3 is a model of the crystalized structure of HIV-Rev NES (left) and the crystalized structure of the PKI alpha NES (right). Critical residues required for nuclear export are labeled in black. The image was created using UCSF Chimera.

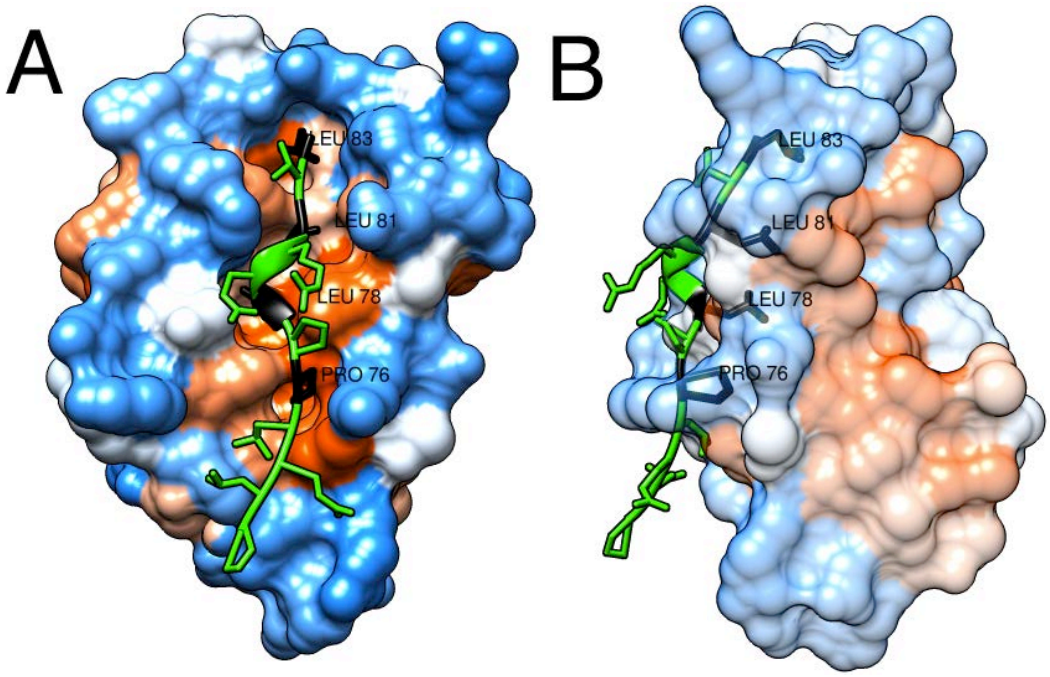

Figure 4: The crystalized structure of HIV-Rev bound to CRM1 binding pocket
The .pdb file containing the HIV-1 Rev NES-CRM1-RanGTP nuclear export complex was obtained from the protein data bank, access code 3NBZ. The well documented nuclear export sequence found in HIV-Rev was crystalized bound to CRM1. As depicted critical residues in HIV-Rev (shown in black) occupy the spatial arrangement necessary for binding to the CRM1 active pocket. (A) Frontal view of the protein binding interaction. (B) Side view of the protein binding interactions. Models were generated using UCSF Chimera.

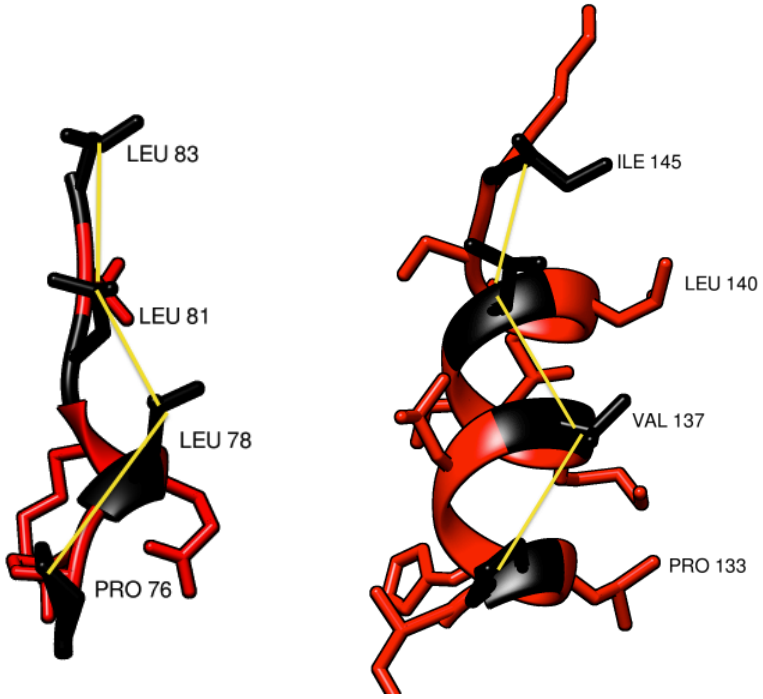

Figure 5: Positioning of critical residues in HIV-Rev and PCV1
HIV-Rev NES (left) with critical residues in black shows a similar amino acid arrangement to the proposed NES located in the Tail region of PCV1 (right). The proposed critical residues are displayed in black and are shown to occupy the same arrangement as those found in HIV-Rev. The image was created using UCSF Chimera.

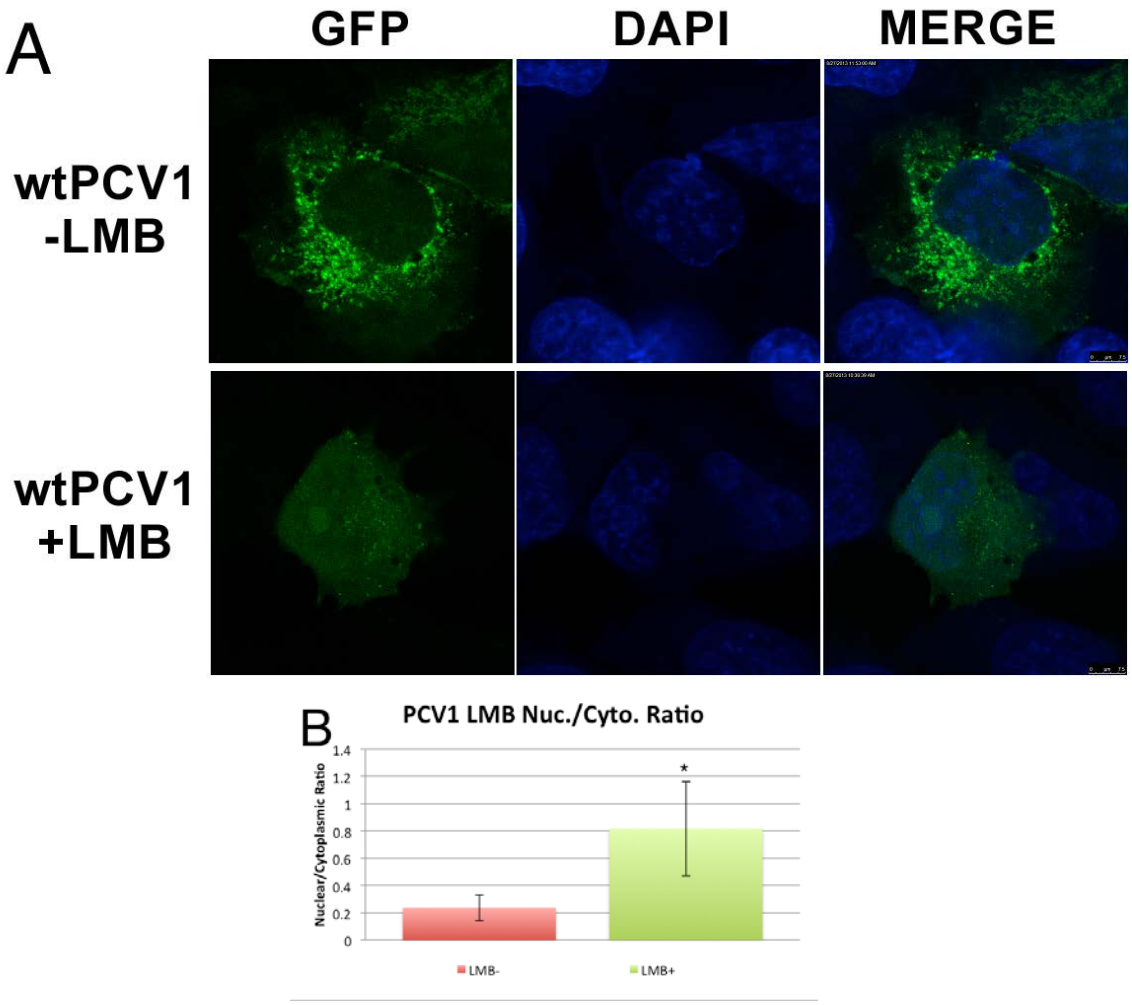

Figure 6 Fluorescent microscopy of PCV1 VP3 shows the presence of LMB sensitive nuclear export sequence

(A) H1299 cells were transfected with wild type PCV1 VP3 using an Effectene Kit (Qiagen). Twenty-four hours post transfection leptomycin B was added, cells were fixed and imaged under confocal microscopy. Upon addition of LMB nuclear accumulation can be seen. (B) The nuclear/cytoplasmic ratio was calculated to quantify the fluorescence of the images taken under confocal microscopy. Using the corrected total cell fluorescence the intensity of GFP fluorescence found in the nucleus of three representative cells was divided by the intensity of GFP fluorescence found in the cytoplasm. This established the nuclear/cytoplasmic ratio of GFP expression. This was performed for cells treated with LMB and cells in the absence of LMB. Statistical analysis shows results to be significant (*P=0.047).

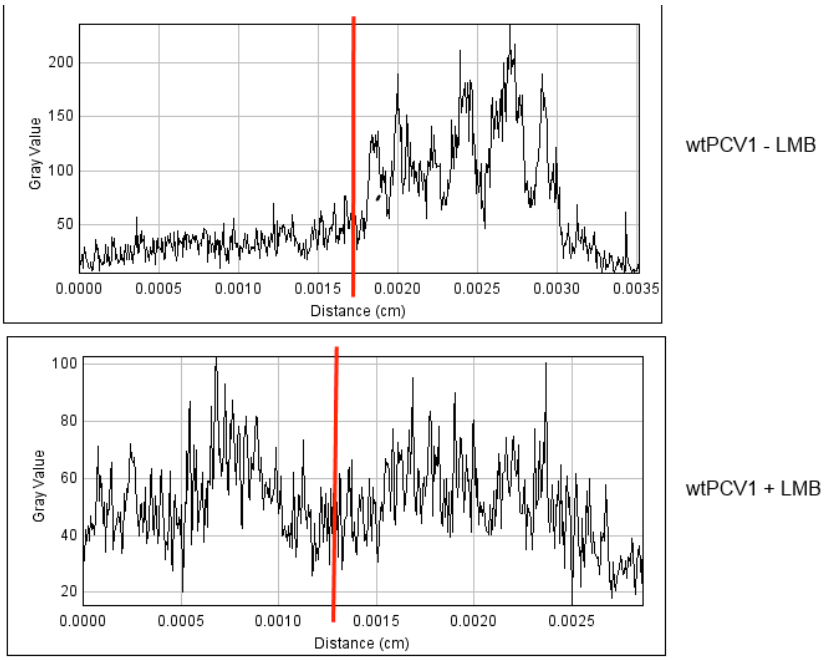

Figure 7: Brightness intensity detailing GFP expression in H1299 cells

Image J was used to create a brightness intensity graph to graphically determine the pixel intensity of GFP fluorescence. The intensity was measured from the inner nuclear membrane to the outer cell membrane. Right of the red lines represents cytoplasmic and left represents nuclear. The graph was made using the representative cell in the absence of LMB (top), showing the highest intensity in the cytoplasm (right). The graph of the representative cell treated with LMB (bottom), shows a diffuse intensity suggesting an equal distribution of fluorescence in the nucleus (left) and cytoplasm (right).

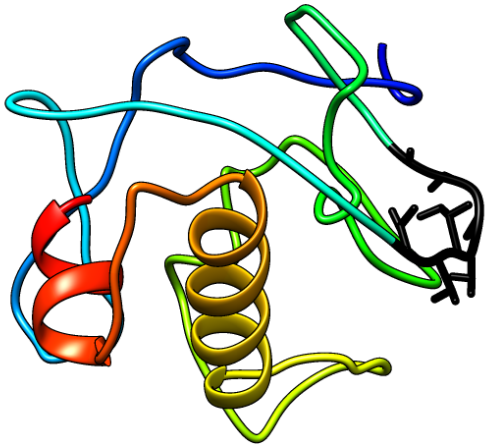

Figure 8: 3D Prediction of Apoptin from I-TASSER server with Leucine 44 & 46 mutated to Alanine

The point mutation of leucines 44 and 46 in Apoptin is known to completely remove its export capability. Interestingly, this mutation also completely changes the conformation of the protein, completely exposing the NES region. Apoptin's NES region (residues 40-46) is shown in black. The model was generated using UCSF Chimera.

References

1. Adair, B. (2000). Immunopathogenesis of Chicken Anemia Virus Infection. *Developmental and Comparative Immunology, 24*, 9.
2. Argiris, K., Panethymitaki, C., & Tavassoli, M. (2011). Naturally occurring, tumor-specific, therapeutic proteins *Experimental Biology and Medicine, 236*, 524-536.
3. Belyi, V., Levine, A., Skalka, A.M., (2010), Sequences from Ancestral Single Stranded DNA Viruses in Vertebrate Genomes: the Parvoviridae and Circoviridae are more than 40 to 50 Million Years Old. *Journal of Virology, 84(23)*, 12458-12462.
4. Bourque, J., & Goldstein, J. (2008). Cloning and Structure-Function Analysis of Porcine Circovirus 2 VP3: Worcester Polytechnic Institute.
5. CASP, & Prediction, C. A. o. T. f. P. S. (2012). 10th Community Wide Experiment on the Critical Assessment of Techniques for Protein Structure Prediction. 2013, from http://predictioncenter.org/casp10/
6. Chaiyakul, M., Hsu, K., Dardari, R., Marshall, F., & Czub, M. (2010). Cytotoxicity of ORF3 Proteins from a Nonpathogenic and a Pathogenic Porcine Circovirus. *Journal of Virology, 84*(21), 8.
7. Cheng, J.-H., Sheu, S.-C., Lien, Y.-Y., Lee, M.-S., Chen, H.-J., Su, W.-H., & Lee, M.-S. (2012). Identification of the NLS and NES Motifs of VP2 from Chicken Anemia Virus and the Interaction of VP2 with Mini-Chromosome Maintenance Protein 3. *Veterinary Research*, 12.
8. Chipuk, J. E., & Green, D. R. (2008). How do BCL-2 proteins induce mitochondrial outer membrane permeabilization? *Trends Cell Biol. , 18*(4), 157-164.
9. Clancey, S., & Mahoney, B. (2013). Assessment of Functionality of Nuclear Export Sequences in Porcine Circovirus 1 VP3: Worcester Polytechnic Institute.
10. Conerly, P., & McShea, M. (2009). Cloning and Expression of PCV1 ORF3: Worcester Polytechnic Institute.
11. Danen-Van Oorschot, A. A., EB, V. D. A. J., & Noteborn, M. H. M. (2000). The Chicken Anemia Virus-Derived Protein Apoptin Requires Activation of Caspases for Induction of Apoptosis in Human Tumor Cells. *JOURNAL OF VIROLOGY 74*(15), 7072-7078.
12. Danen-van Oorschot, A. A., Fischer, D., Grimbergen, J., Klein, B., Zhuang, S.-M., Falkenburg, J., Noteborn, M. (1997). Apoptin induces apoptosis in human transformed and malignant cells but not in normal cells. *PNAS, 94*, 5843-5847.
13. Danen-Van Oorschot, A. A., Zhang, Y., Leliveld, S., Rohn, J., & Mumberg, D. (2003). Importance of Nuclear Localization of Apoptin for Tumor-Specific Induction of Apoptosis. *Journal of Biological Chemistry, 278*, 8.
14. Das, R., Qian, B., Raman, S., Vernon, R., Thompson, J., Bradley, P., Baker, D. (2007). Structure prediction for CASP7 targets using extensive all-atom refinement with Rosetta@home. *Proteins: Structure, Function, and Bioinformatics, 69*, 118-128.

15. Fu, S., Imai, K., & Horton, P. (2011). Prediction of Leucine-Rich Nuclear Export Signal Containing Proteins with NESsential. *Nucleic Acids Research, 39*(16), 12.
16. Gagnon, C., Tremblay, D., Tijssen, P., Venne, M.-H., Houde, A., & Elahi, S. M. (2007). The Emergence of Porcine Circovirus 2b Genotype (PCV-2b) in Swine in Canada.
17. Ghobrial, I. M., Witzig, T. E., & Adjei, A. A. (2005). Targeting Apoptosis Pathways in Cancer Therapy. *A Cancer Journal for Clinicians, 55*, 178-194.
18. Harding, J. (2007). History of Porcine Circoviral Disease (PCVD) and Current Western Canadian Situation.
19. Heckl, S., Regenbogen, M., Sturzu, A., Gharabaghi, A., Feil, G., Beck, A., Nagele, T. (2008). Value of Apoptin's 40-Amino-Acid C-Terminal Fragment for the Differentiation Between Human Tumor and Non-Tumor Cells. *Apoptosis*, 13.
20. Heilman, D. W., Teodoro, J. G., & Green, M. R. (2006). Apoptin Nucleocytoplasmic Shuttling Is Required for Cell Type-Specific Localization, Apoptosis, and Recruitment of the Anaphase-Promoting Complex/Cyclosome to PML Bodies. *Journal of Virology, 80*(15), 7535-7545.
21. Huo, D.-H., Yi, L.-N., & Yang, J. (2008). Interaction with Ppil3 leads to the cytoplasmic localization of Apoptin in tumor cells. *Biochemical and Biophysical Research Communications, 372*, 14-18.
22. Jiang, X., & Wang, X. (2004). CYTOCHROME *C-MEDIATED* APOPTOSIS *Annu. Rev. Biochem. , 73*, 87-106.
23. Kokolis, J., & Spada, L. (2010). Assessing the Functionality of Localization Sequences Isolated from PCV1 VP3: Worcester Polytechnic Institute.
24. Kucharski, T. J., Gamache, I., Gjoerup, O., & Teodoro, J. G. (2011). DNA Damage Response Signaling Triggers Nuclear Localization of the Chicken Anemia Virus Protein Apoptin. *JOURNAL OF VIROLOGY, 85*(23), 12638–12649
25. Leber, B., Lin, J., & Andrews, D. W. (2007). Embedded together: The life and death consequences of interaction of the Bcl-2 family with membranes. *Apoptosis, 12*, 897-911.
26. Lee, J., Wu, S., & Zhang, Y. (2009). Ab Initio Protein Structure Prediction. *From Protein Structure to Function with Bioinformatics*(1), 1-26.
27. Lee, Y., Cheng, C., Chang, Y., Wang, T., & Yuo, C. (2007). Apoptin T108 phosphorylation is not required for its tumor-specific nuclear localization but partially affects its apoptotic activity. *Biochem Biophys Res Commun., 354*(2), 391-395.
28. Leliveld, S. R., Dame, R. T., Mommaas, M. A., Koerten, H. K., Wyman, C., Danen-van Oorschot, A. A. A. M., . . . Abrahams, J. P. (2003). Apoptin protein multimers form distinct higher-order nucleoprotein complexes with DNA. *Nucleic Acids Research, 31*(16), 4805-4813
29. Leliveld, S. R., Dame, R. T., Rohn, J. L., Noteborn, M. H. M., & Abrahams, J. P. (2003). Apoptin's functional N- and C-termini independently bind DNA *FEBS Letters, 557*, 155-158.

30. Leliveld, S. R., Zhang, Y.-H., Rohn, J. L., & Noteborn, M. (2003). Apoptin Induces Tumor-specific Apoptosis as a Globular Multimer *THE JOURNAL OF BIOLOGICAL CHEMISTRY, 278*(11), 9042–9051
31. Li, Z., & Scheraga, H. A. (1987). Monte Carlo-minimization approach to the multiple-minima problem in protein folding. *PNAS, 84*, 6611-6615.
32. Liang, Y., Lin, S.-Y., Brunicardi, F. C., Goss, J., & Li, a. K. (2008). DNA Damage Response Pathways in Tumor Suppression and Cancer Treatment. *Official Journal of the International Society of Surgery*.
33. Liu, J., Chen, I., Du, Q., Chua, H., & Kwang, J. (2006). The ORF3 Protein of Porcine Circovirus Type 2 is Involved in Viral Pathogenesis In Vivo. *Journal of Virology*.
34. Liu, J., Chen, I., & Kwang, J. (2005). Characterization of a Previously Unidentified Viral Proten in Porcine Circovirus Type 2-Infected Cells and Its Role in Virus-Induced Apoptosis. *Journal of Virology, 79*(13).
35. Liu, J., Zhu, Y., Chen, I., Lau, J., He, F., Lau, A., Kwang, J. (2007). The ORF3 Protein of Porcine Circovirus Type 2 Interacts withPorcine Ubiquitin E3 Ligase Pirh2 and Facilitates p53Expression in Viral Infection. *Journal of Virology, 81*(17), 8.
36. Maddika, S., Bay, G. H., Kroczak, T. J., Ande, S. R., Maddika, S., Wiechec, E., Los, M. (2007). Akt is transferred to the nucleus of cells treated with apoptin, and it participates in apoptin-induced cell death. *Cell Prolif., 40*, 835–848
37. Maddika, S., Booy, E. P., Johar, D., Gibson, S. B., Ghavami, S., & Los, M. (2005). Cancer-specific toxicity of apoptin is independent of death receptors but involves the loss of mitochondrial membrane potential and the release of mitochondrial cell-death mediators by a Nur77-dependent pathway. *Journal of Cell Science, 118*(19), 4485-4493.
38. Maddika, S., Panigrahi, S., Wiechec, E., Wesselborg, S., Fischer, U., Schulze-Osthoff, K., & Los, M. (2009). Unscheduled Akt-Triggered Activation of Cyclin-Dependent Kinase 2 as a Key Effector Mechanism of Apoptin's Anticancer Toxicity. *MOLECULAR AND CELLULAR BIOLOGY, 29*(5), 1235–1248
39. Maddika, S., Wiechec, E., Ande, S. R., Poon, K., Fischer, U., Wesselborg, S., Los, M. (2008). Interaction with PI3-kinase contributes to the cytotoxic activity of Apoptin. *Oncogene, 27*, 3060–3065
40. Mankertz, A., Caliskan, R., Hattermann, K., Hillenbrand, B., Kurzendoerfer, P., Mueller, B., Finsterbusch, T. (2004). Molecular Biology of *Porcine Circovirus*: Analyses of Gene Expression and Viral Replication. *Veterinary Microbiology*.
41. Noteborn, M. (2004). Chicken Anemia Virus Induced Apoptosis: Underlying Molecular Mechanisms. *Veterinary Microbiology, 98*, 6.
42. Noteborn, M., Todd, D., Verschueren, C., de Gauw, H., Curran, W., Veldkamp, S. Koch, G. (1994). A single Chicken Anemia Virus Protein Induces Apoptosis. *Journal of Virology, 68*(1), 6.
43. Peters, J.-M. (2006). The anaphase promoting complex/ cyclosome: a machine designed to destroy. *Nature Publishing Group 7*, 644-656.

44. Peters, M., Jackson, D., Crabb, B., & Browning, G. (2002). Chicken Anemia Virus VP2 is a Novel Dual Specificity Protein Phosphatase. *The Journal of Biological Chemistry, 277*(42), 9.
45. Poon, I. K. H., Oro, C., Dias, M. M., Zhang, J., & Jans, D. A. (2005). Apoptin Nuclear Accumulation is Modulated by a CRM1-Recognized Nuclear Export Signal that is Active in Normal but not in Tumor Cells. *Cancer Res., 65*, 7059-7064
46. Rogers, A., & Hough, K. (2012). The Effect of Subcellular Localization on the Oncopathogenic Capability of Porcine Circovirus Type 1 VP3: Worcester Polytechnic Institute.
47. Rohn, J. L., Zhang, Y.-H., Aalbers, R. I. J. M., Otto, N., Den Hertog, J., Henriquez, N. V., . . . Noteborn, M. H. M. (2002). A Tumor-specific Kinase Activity Regulates the Viral Death Protein Apoptin. *THE JOURNAL OF BIOLOGICAL CHEMISTRY, 277*(52), 50820-50827.
48. Rosenberger, J., & Cloud, S. (1998). Chicken Anemia Virus. *Poultry Science, 77*, 3.
49. Sancar, A., Unsal-Kacmaz, K., Lindsey-Boltz, L. A., & Linn, S. (2004). Molecular Mechanisms of Mammalian DNA Repair and the DNA Damage Checkpoints. *Annual Reviews in Biochemistry, 73*, 39-85.
50. Smyth, J., Moffett, D., McNulty, M., Todd, D., & Mackie, D. (1993). A Sequential Histopathologic and Immunocytochemical Study of Chicken Anemia Virus Infection at One Day of Age *Avian Diseases, 37*(2), 15.
51. Teceno, N. (2013). Investigating Porcine Circovirus Type 2 Viral Protein 3 Multimerization Capabilities (pp. 34): Worcester Polytechnic Institute.
52. Teodoro, **J. G.**, Heilman, D. **W.**, **P**arker, A. **E.**, & **Gr**een, M. **R.** (2004). The viral protein Apoptin associates with the anaphase-promoting complex to induce G2/M arrest and apoptosis in the absence of p53. *Genes Dev, 18*, 1952-1957
53. Thachuk, C., Shmygelska, A., & Hoos, H. H. (2012). A Replica Exchange Monte Carlo Algorithm for Protein Folding in the HP Model. *BMC Bioinformatics*.
54. Thornton, B. R., Ng, T. M., Matyskiela, M. E., Carroll, C. W., Morgan, D. O., & Toczyski, D. P. (2006). An architectural map of the anaphase-promoting complex. *Genes & Development 20*, 449-460
55. Thornton, B. R., & Toczyski, D. P. (2003). Securin and B-cyclin/CDK are the only essential targets of the APC. *Nature Cell Biology, 5*(12), 1090-1094.
56. Tischer, I., Rasch, R., & Tochtermann, G. (1974). Characterization of Papovavirus- and Picornavirus-Like Particles in Permanent Pig Kidnet Cell Lines.
57. Van Leuken, R., Clijsters, L., & Wolthuis, R. (2008). To cell cycle, swing the APC/C *Biochimica et Biophysica Acta 1786*, 49-59.
58. Xu, D., & Zhang, Y. (2012). Ab initio protein structure assembly using continuous structure fragments and optimized knowledge-based force field. *Proteins*(80), 1715-1735.
59. Yuasa, N., Taniguchi, T., & Yoshida, I. (1979). Isolation and Some Characteristics of an Agent Inducing Anemia in Chicks. *Avian Diseases, 23*(2), 20.

60. Zhou, B.-B. S., & Elledge, S. J. (2000). The DNA damage response: putting checkpoints in perspective. *Nature, 408*, 433-439.
61. Zhuang, S.-M., Shvarts, A., Ormondt, H. v., Jochemsen, A., Eb, A. v. d., & Noteborn, M. (1995). Apoptin, a Protein Derived from Chicken Anemia Virus, Induces p53-independentApoptosis in Human Osteosarcoma Cells. *Cancer Research*, 4.